Fe-Heme Conformations in Ferric Myoglobin

S. Della Longa,* S. Pin,# R. Cortès,§ A. V. Soldatov,¶ and B. Alpert#

*Dept. Medicina Sperimentale and INFM, Università dell'Aquila, I-67100 L'Aquila and Ist. Naz. Fisica Materia (INFM), Italy; #Lab. de Biologie Physico-Chimique, Univ. F-75231 Paris VII, France; §LURE, CNRS CEA MEN, Univ. Paris Sud, F-91045 Orsay, France; and ¶Department of Solid State Physics, Rostov State University, 344090 Rostov-on-Don, Russia

ABSTRACT X-ray absorption near-edge structure (XANES) spectra of ferric myoglobin from horse heart have been acquired as a function of pH (between 5.3 and 11.3). At pH = 11.3 temperature-dependent spectra (between 20 and 293 K) have been collected as well. Experimental data solve three main conformations of the Fe-heme: the first, at low pH, is related to high-spin aquomet-myoglobin (Mb^+OH_2). The other two, at pH 11.3, are related to hydroxymet-myoglobin (Mb^+OH^-), and are in thermal equilibrium, corresponding to high- and low-spin Mb^+OH^-. The structure of the three Fe-heme conformations has been assigned according to spin-resolved multiple scattering simulations and fitting of the XANES data. The chemical transition between Mb^+OH_2 and high-spin Mb^+OH^-, and the spin transition of Mb^+OH^-, are accompanied by changes of the Fe coordination sphere due to its movement toward the heme plane, coupled to an increase of the axial asymmetry.

INTRODUCTION

The study of the active site structure of the hemoprotein, and its variations on ligand binding, is a key step in solving problems of carriage and storage of molecular oxygen, and in general to gain an understanding of the relationship between protein structure and function. The properties of methemoglobin and metmyoglobin, which have a heme iron in the ferric form, are widely studied. The heme iron in these ferric hemoproteins is hexacoordinated, with a water molecule as its sixth ligand. The H_2O group can be ionized to OH^- or reversibly exchanged with other ligands, e.g., N_3^-, CN^-, F^-. In all cases, the sixth ligand change in ferric hemoproteins is accompanied by variations of the magnetic and structural properties of the heme iron coordinated complex: these variations are similar to those observed during the oxygenation process of deoxyhemoproteins to oxyhemoproteins.

In ferrihemoglobin (Hb^+) and ferrimyglobin (Mb^+), it is known that the Fe-heme has an intermediate value of magnetic susceptivity between 5.92 μ_B, characteristic of five unpaired electrons, and 2.24 μ_B, characteristic of one unpaired electron, this value fluctuating depending on pH and temperature, and being different for Mb^+ and Hb^+ (Kotani, 1968). This fact is attributed to the presence of two magnetic isomers, one in a high-spin (HS) and the other in a low-spin (LS) state, and the measured temperature dependence of the paramagnetic susceptivity is assumed to behave according to a Boltzmann distribution between the two states (Iizuka and Kotani, 1969). Mb^+s and Hb^+s undergo an acid-alkaline transition between the aquomet and hydroxymet forms with pK′ values ranging between 8 and 9, the higher value pertaining to Mb^+. The paramagnetic susceptivity in Hb^+ was found to variate as a function of pH (Kotani, 1968; Yonetani et al., 1971), giving evidence of an LS adduct at room temperature. It changes from 5.77 μ_B at pH = 6–7 (corresponding to 95% HS) to 4.4 μ_B at high pH values (48% HS). It is well established that the pH dependence in Mb^+ is more limited (5.1 μ_B at high pH values, 70% HS) (Beetlestone and George, 1964). Mb^+OH^- at pH 11.3 converts completely to LS by cooling at low temperature (below T = 100 K). Despite the large body of knowledge, one must compare these data and more recent investigations with caution, because the spin state of the Fe-heme is likely to depend also on the protein environment (buffer, ionic strength), that has evolved in time with the preparation protocols.

However, the conformational landscape of Fe-heme in Hb^+ and Mb^+ under environmental parameters, e.g., pH and temperature, is not so well defined. It is obvious to expect changes of the Fe-heme local structure consequent to either acid-alkaline transition or spin transition at high pH values. Titration of distal histidine must directly influence the coordination geometry of the sixth iron ligand. Moreover, the iron LS → HS transition is believed to be accompanied by a displacement of the iron along the heme normal as a consequence of either the metal-pyrrol nitrogen repulsion resulting from the b_{1g} ($d_{x^2-y^2}$) antibonding molecular orbital (Perutz et al., 1968; Perutz, 1979), or pseudo Jahn-Teller distortion coupling of the $a_{2u}(\pi)$ porphyrin orbital to the $d^2_{z^2-\sigma}$ Fe–N_ϵ antibonding orbital (Bersuker and Stavrov, 1988). However, x-ray diffraction (XRD) experiments probe an average structure of the Fe-heme at the crystal conditions, and do not probe the Fe spin state. The XRD data on sperm whale Mb^+ (Takano, 1977), reporting an Fe-heme displacement of 0.4 Å toward the proximal histidine, are in contrast with that on horse Mb^+ (Evans and Brayer, 1990), reporting in-plane Fe. Other techniques applied to study the spin/structure problem add poor structural

Received for publication 26 February 1998 and in final form 17 August 1998.

Address reprint requests to S. Della Longa, Dip. Medicina Sperimentale, Universita' dell'Aquila, Via Vetoio, 67100 loc. Coppito, L'Aquila, Italy. Tel.: +39-862-433568; Fax: +39-862-433523; E-mail: dellalonga@vaxaq.cc.univaq.it.

0006-3495/98/12/3154/09 $2.00

information: UV/V spectra are very sensitive to the π-electron density changes inside the heme, but are poorly sensitive to the axial symmetry; the structural interpretation of temperature-dependent data is even more complicated because of strong vibrational coupling (Eaton and Hofrichter, 1981). Electron paramagnetic spectroscopy (EPR) can reveal structural details only at low temperatures (Yonetani et al., 1971). Resonance Raman spectroscopy is very sensitive to the Fe-heme arrangement, but the fifth and sixth iron ligand geometries remain elusive: an Fe-His stretching vibration has been assigned unambiguously only in deoxy-Mb (at $\approx$220 cm^{-1}); a resonance Raman peak (in the range 490–500 cm^{-1}) has been assigned to the Fe–O stretching frequency in aquomet-myoglobin (Asher and Shuster, 1979): the observed 5 cm^{-1} shift between Hb^+OH^- (495 cm^{-1}) and Mb^+OH^- (490 cm^{-1}) was interpreted as an Fe–O bond length increasing only 0.01 Å, but the correlation between Raman frequency shifts and bond length changes are questioned.

An X-ray absorption spectroscopy (XAS) investigation of the pH and temperature dependence of ferric hemoproteins gives complementary information to approach this problem. In fact,

1. The x-ray absorption near-edge structure (XANES) (Pin et al., 1994a) and extended x-ray absorption fine structure (EXAFS) (Chance et al., 1996) signals probe the average structure of the Fe site of the protein in solution at any environmental conditions (pH, temperature, solvent), exhibiting different Fe-heme conformations if their conformational equilibria are opportunely modulated to obtain each of their different specific states. It is just the case of aquomet-myoglobin when both pH and temperature are changed in solution. However, EXAFS in the single scattering regime could hardly probe conformational changes related to a little displacement of the Fe with respect to the heme plane. For example, in the EXAFS study of the high affinity-low affinity transition in carp HbCO (Chance et al., 1986), no difference in the iron first-shell average distance were found to accompany the transition. The same authors, by looking at the range 7140–7200 eV (including the multiple scattering regime) that they called LFIR, i.e., ligand field indicator region, observed changes interpreted resulting from the Fe displacement. Therefore, further information can be provided by the analysis of multiple scattering (MS) components in XAS.

2. Nuclear vibrations induce exponential damping terms in the energy (or electron wavenumber, k) scale of an XAS spectrum. For a certain absorber-scatterer couple at a distance R_j, this damping factor in the single scattering regime is accounted for by the Debye-Waller term $[\exp(-2\sigma_j^2k^2)]$; where σ_j is the root mean square (RMS) deviation of R_j. It is related to the individual atomic displacements of the absorbing atom ($\langle x_{abs}^2\rangle$) and the scattering atom ($\langle x_{sca}^2\rangle$) by the following relationship:

$$\sigma_j = \langle(\vec{x}_{abs}\cdot\vec{R}_j)^2\rangle + \langle(\vec{x}_{sca}\cdot\vec{R}_j)^2\rangle - 2\langle(\vec{x}_{abs}\cdot\vec{R}_j)(\vec{x}_{sca}\cdot\vec{R}_j)\rangle \quad (1)$$

The last term of Eq. 1 includes correlated motions of the absorber-scatterer couple. The temperature dependence of the individual atomic displacements in Mb^+ is well known, including a thermal transition at $T \approx 200$ K giving evidence for the existence of substates (Hartmann et al., 1982). Nevertheless, the temperature dependence of σ_j is much more limited because of the correlation term (D'Alba et al., 1990). The correlation tends to vanish for further shells, but in disordered systems such as proteins, only a few correlated shells contribute to the XAS signal. Other degrees of freedom in the multiple scattering regime, e.g., rotation angles, neglected in relation (1), could contribute, in principle, to thermal damping. However, experimentally, temperature effects in the XANES range are found to be negligible in LS MbCO (unpublished observation), so it is reasonable to interpret temperature-dependent XANES spectra of Mb^+ without considering effects from nuclear vibrations.

Therefore, a pH- and temperature-dependent XANES study of ferric horse myoglobin has been carried out to get structural information and investigate the main Fe-heme conformations of horse and sperm whale ferric myoglobin. Data support the existence of a multistate equilibrium between HS and LS forms of the Fe-heme. At least three main states corresponding to HS iron in Mb^+OH_2, and HS and LS iron in Mb^+OH^-, have been structurally assigned. The iron spin transition in horse Mb^+OH^- is accompanied by the same spectral changes as observed in sperm whale (Oyanagi et al., 1987). The XANES theory, including spin effects under a self-consistent potential, has been used to extract information on both the atomic and electronic changes at the Fe-heme site (Della Longa et al., 1995, 1998). Solving Fe-heme structural states due to boundary conditions of the protein (essentially its electrostatic field) will be helpful to improve the interpretation of further XANES data concerning the structure of mutants (Pin et al., 1994b), and intermediate conformations in the ligand binding process (Della Longa et al., 1994).

METHODS

Ferric myoglobin solutions were prepared from lyophilized horse heart myoglobin (M-1882, Sigma-Aldrich Chimie S.a.r.l., St. Quentin Fallarier, France) or from lyophilized sperm whale myoglobin purchased before the ban on whaling. After an overnight dialysis (at 4°C) against distilled water, the different pH values of myoglobin samples were obtained by dialysis (48 h at 4°C), against 100 mM potassium (pH 5.0, 7.0, 9.0, or 11.5). The pH values were not readjusted to keep the same ionic strength, but were controlled for all samples. In these conditions, the pH values for horse myoglobin samples were 5.3, 7.0, 8.7, and 11.3; whereas the values for sperm whale samples were 6.9 and 11.1. Samples were concentrated by passing on an Amicon Centricon 10. The protein concentrations were calculated from the absorbance at the isobestic points (Antonini) and the values were between 7 and 11 mM for horse myoglobin samples, and 3 mM for sperm whale myoglobin samples. Each sample was centrifuged at 45,000 $\times$ g before each XAS measurement. A control procedure on possible radiation damage was made by visible absorption measurements on the XANES samples. The absorption spectra on a DMS 100 Varian spectrophotometer (from 450 to 650 nm) were identical for the samples before and after their x-ray exposition. Moreover, each XANES spectrum

was collected by scans, and before averaging the scans it was verified that the last scan was identical to the first one.

Fe K-edge x-ray absorption spectra were collected in fluorescence mode at the beam line D21 of the LURE synchrotron facility by using an energy-resolving array detector made by 7 Ge elements of very high purity from CANBERRA industries. The energy resolution at the Fe K_α fluorescence (6400 eV) was 170 eV. An Si(311) double crystal used as a channel cut was adopted as a monochromator, and the spectral resolution at the Fe K-edge was ~1 eV. Harmonic contamination was rejected by using a total reflection mirror after the monochromator. The spectra (4 frames about 601 experimental points with a $\Delta E = 0.2$ eV) have a total signal averaging of 32 s/point. The fluorescence counts jumped from 70 counts/s/element before the edge (7100 eV), to ~850 counts/s/element above the edge (7250 eV), giving a total count jump of ~175,000 with a noise-to-signal ratio of $6 \cdot 10^{-4}$ before the edge and $2 \cdot 10^{-3}$ after the edge. In all experimental spectra presented here, the energy is aligned at the absorption threshold of metallic Fe foil. XANES spectra have been collected at pH = 5.3, 7, 8.7, and 11.3 for horse Mb, and to pH 6.9 and 11.1 for sperm whale Mb. The temperature-dependent experiment has been carried out independently. Another sample at pH 11.3 has been cooled down to 20 K by using a liquid helium cryostat (model 22C Cryodine Cryocooler by CT Cryogenics, temperature controller model 80S by Lake Shore Cryotronics, and silicon diode temperature sensor DT-470-SD by Lake Shore). Then, temperature-dependent spectra were consecutively acquired at $T = 20$, 100, 150, 220, and 293 K after stabilization of temperature. The last spectrum of the sample has been compared with the fresh sample measured at room temperature in the pH-dependence experiment to check for any experimental protocol condition giving systematic errors. The two spectra, after background subtraction and normalization, are identical within statistical counts. The fit goodness F in every fitting procedure is calculated as

$$F = \frac{1}{N\sigma^{\exp}} \sqrt{\sum_{i=1}^{N} (y_i^{\text{fit}} - y_i^{\exp})^2}$$

where N is the number of fitted experimental points, $\sigma^{\exp}$ is the noise-to-signal value, and y_i^{fit} and $y_i^{\exp}$ are theoretical and experimental absorption values, respectively.

The XANES simulations make use of the one-electron full multiple scattering formalism (Durham et al., 1982), included in the G4XANES computer package developed by us (Della Longa et al., 1995). The calculations have been performed in the real space for a three-shell cluster in the same manner as previous works (Bianconi et al., 1985; Della Longa et al., 1993), where we did not consider the spin state. For a chosen structure of the Fe-heme cluster, spin-resolved XANES spectra can be calculated corresponding to the HS or LS configuration of the absorbing Fe atom, as described previously (Della Longa et al., 1998). A broadening Lorentzian function is applied to the calculated XANES to take into account the core hole lifetime (1.2 eV), the experimental resolution (1.0 eV), and an energy-dependent factor representing the photoelectron lifetime due to inelastic scattering by valence electrons. The energy-dependent part is zero below the Fermi energy and contains jumps at the energies of plasmon excitations. Plasmon energies and jumps have been initially chosen consistently to values reported on electron energy loss spectra (EELS) of Fe borides (Bratkovsky et al. 1994), then adjusted to fit the experimental data. The energy zero of the simulation is the theoretical average potential energy between atomic Muffin Tin spheres, VMT.

The basic cluster used for the multiple scattering (MS) simulations has no symmetry, including 32 atoms from the porphyrin ring, the proximal histidine, and the sixth ligand. Despite the great number of degrees of freedom, a large body of knowledge (essentially from crystallography and EXAFS) furnish ancillary information allowing selection of a limited number of parameters at the Fe-heme site, which can affect the XANES. The Fe-heme system has a pseudo-C_{4v} symmetry; the histidine ring and pyrrol rings of the porphyrin are retained perfectly rigid. We have selected the following parameters: 1) d(Fe–N_p) (i.e., the equatorial first shell average distance from the pyrrol nitrogens in a C_{4v} symmetry); 2) and 3) d(Fe–Nϵ) and d(Fe–O) (the axial distances of the proximal histidine and the sixth ligand); 4) and 5) the rotation (tilting) angles of the same axial ligands; 6) the azimuthal angle of the proximal histidine; 7) the Fe displacement along the heme normal; 8) the heme "doming" (i.e., in-phase rotation of the four pyrrol rings, affecting in turn the equatorial first shell average distance); 9) the heme "ruffling" (i.e., opposite rotation of the two couples of opposite pyrrol rings, affecting the in-phase scattering of the equatorial ligands). Heme doming was changed in concert with the Fe-heme displacement, the Fe–N_p distance being constrained between 2.007 and 2.027 Å, so that a unique generalized coordinate took these parameters into account. The validity of this assumption could be confirmed by EXAFS, as in the case of carp HbCO (little changes in the Fe–N_p distance, unrelated to Fe displacement and heme doming, being also possible). A Monte Carlo search has been adopted to simulate the experimental data among these reduced degrees of freedom. Hundreds of random Fe-heme structures have been generated to fit each experimental spectrum, taking about six weeks of elapsed time per search on an IBM-RISC 6000. Because these severe computational limits restrain the number of trials, the refinement of minimal search has been attempted only four times, by reducing each parameter interval proportionally to the fit improvement, similarly to the procedure used in optimization by simulated annealing (Kirkpatrick et al., 1983). As a consequence it is still not possible to attempt a full optimization or, in turn, a complete statistical analysis. A correlation analysis on the entire set of independent parameters would be helpful to solving the problem of finding a uniqueness of the parameter fitting by allowing one to determine how much the value of one parameter depends on the evaluation of other parameters (as in the case of coordination number and Debye-Waller factor in EXAFS analysis). However, rather than to increase the number of independent parameters in the actual calculation procedure (by treating, for example, the Fe-N_p distance, the Fe displacement and heme doming as independent parameters), the only strategy that can be used to get new results in reasonable time seems to be in writing a new XANES code for parallel computing. The implementation of a XANES simulation software in parallel computing systems including a full statistical analysis is in progress in our laboratory. For the moment, it seems reasonable to evaluate bond distances as average among values found within an allowable error of 10^{-3} above the minimum of the Fit Index, Min(F), a certainly upper limit for the sensitivity of the method (as shown in Results and Fig. 5). Statistical errors can be estimated as well, as half-maximum dispersion among these values.

One has to apply the XANES theory keeping in mind that systematic errors can arise essentially because of 1) the basic approximations in using the one-electron theory and spherically averaged atomic muffin tin potentials; and 2) different conformational substates at the metal site could exist (Parak et al., 1987; Frauenfelder et al., 1988; Doster et al., 1989). The XANES spectra in such a case probe the metal site structure averaged over the protein ensemble, being close to a particular conformation only if it has a high probability.

RESULTS

Experimental data

The Fe K-edge XANES spectra of horse ferric myoglobin at pH 5.3 at $T = 293$ K (*top curve*), pH 11.3 at $T = 293$ K (*middle curve*), and pH 11.3 at $T = 100$ K (*bottom curve*) are depicted in Fig. 1 *A*. Various features of the spectra, P (7111 eV), A (7120 eV), C (7126 eV), D (7132 eV), and C_2 (≈7140–7150 eV), evolve as a function of pH and temperature. The top curve represents aquomet-myoglobin (Mb^+OH_2). The XANES evolution between pH 5.3 and pH 11.3 follows the well-known acid-alkaline transition probed by visible absorption spectroscopy (Antonini and Brunori, 1971): at high pH values the iron sixth ligand position is occupied by an OH^- ion instead of OH_2. Therefore, the middle curve of Fig. 1 *A* represents hydroxymet-myoglobin (Mb^+OH^-). It has also been proposed that the sixth ligand

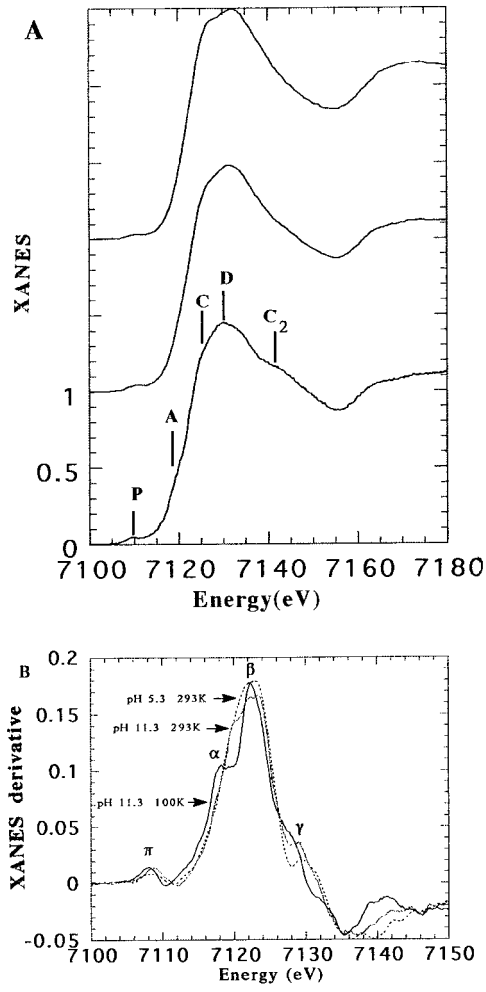

FIGURE 1 (*A*) Fe K-edge XANES spectra of Mb^+OH_2 (pH 5.3, 293 K; *top curve*), and Mb^+OH^- (pH 11.3, 293 K; *middle curve*; pH 11.3, T = 100 K; *bottom curve*). (*B*) XANES derivative spectra of the same spectra.

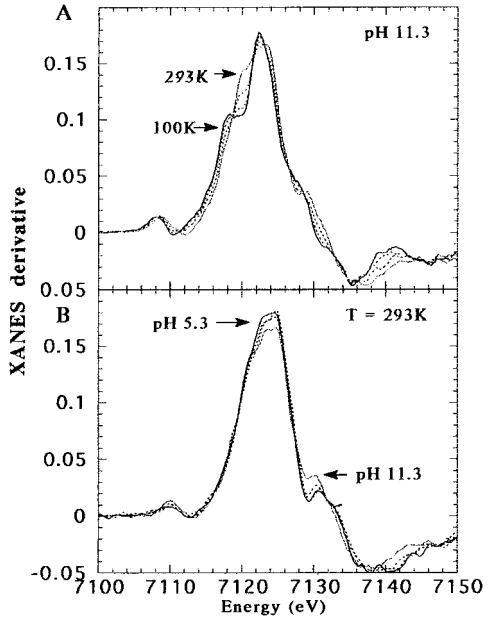

FIGURE 2 (*A*) Temperature dependence of the XANES derivative spectrum of alkaline Mb^+OH^- (pH 11.3, T = 293, 220, 150, and 100 K). (*B*) pH dependence of XANES derivative spectra of Mb^+.

is always OH^-, the acid-alkaline transition corresponding to proton titration of the distal histidine hydrogen bonded to the OH^- ion (Caughey, 1967). The bottom curve of Fig. 1 *A* represents Mb^+OH^- at low temperature, showing marked differences relative to the same sample at room temperature. The XANES derivative spectra of Mb^+OH^- at high and low temperature (pH 11.3 at T = 293 and 100 K) and the spectrum of Mb^+OH_2 (pH 5.3 at T = 293 K) are plotted in Fig. 1 *B*.

The temperature dependence of the XANES derivative spectrum of Mb^+OH^- (pH 11.3 at T = 293, 220, 150, and 100 K) is shown in Fig. 2 *A*. At least six isobestic points are discernible between T = 100 K and T = 293 K, giving the clearest experimental evidence for a two-state thermal equilibrium. The temperature dependence of horse Mb^+OH^- is in full agreement with the results reported on sperm whale Mb^+OH^- (Oyanagi et al., 1987). The pH dependence of Mb^+ is depicted in Fig. 2 *B* where XANES spectra at T = 293 K, pH = 5.3, 7, 8.7, and 11.3 are shown. Another spectral evolution is observed, with different (more undefined) isobestic points. By looking back at Fig. 1 *B*, clearly it is not possible to insert the plotted spectra within the same isobestic points, hence they represent (at least) three structural states of the Fe-heme complex related to the multistate equilibrium:

$$\text{high-spin } Mb^+OH_2 \leftrightarrow \text{high-spin } Mb^+OH^- \leftrightarrow \text{low-spin } Mb^+OH^-$$

with the first equilibrium being related to the acid-alkaline transition at room temperature and the second to thermal spin equilibrium in Mb^+OH^-. As it is well known from visible absorption spectroscopy, the acid-alkaline transition is accompanied by a large rearrangement of the heme π-electrons. The implied slight structural modifications are probed by XANES. At pH 11, Mb^+OH^- is in thermal equilibrium between two spin states of the Fe-heme complex, reaching another different conformation. The term "conformations" is used here to indicate main states reached by the Fe-heme depending on external conditions, so it is distinguished from "substates" (Parak et al., 1987; Frauenfelder et al., 1988; Doster et al., 1989) indicating a multiplicity of protein states under the same environment. Whether these main structural states selected under different conditions coincide or not with substates, as suggested for MbCO (Ansari et al., 1987), is a separate question.

Information on spin is extracted from peak P (7111 eV) assigned to the convolution of the $1s \rightarrow 3d(t_{2g})$ and $1s \rightarrow 3d(e_g)$ electron dipole forbidden transitions. The effects of spin transition on peak P were already discussed in detail in Oyanagi et al. (1987), in the case of sperm whale myoglobin. For the present discussion focused on the Fe site

structure, it is sufficient to take peak P as a spin marker. Going from pH 5.3 to pH 11.3, peak P enhances, but remains at the same energy, corresponding to changes in the d–p mixing (due to variations in the geometry of the Fe coordination sphere) under the same spin state. On the contrary, peak P evolves both in energy position and shape following the thermal spin transition at pH 11.3. As shown in Fig. 2 *A*, peak π (related to peak P) red-shifts at low temperature; moreover, the broad feature at ~7122 eV splits into two peaks α and β at 7118 eV and 7122 eV (as well as in sperm whale myoglobin, Oyanagi et al. (1987) and carp azidomethemoglobin, Pin et al. (1989), and feature γ at ~7130 eV, red-shifts at low temperature (it is related to peak C of the absorption spectrum).

In Fig. 3, XANES difference spectra are plotted ideally following the multistate equilibrium depicted above. From top to bottom, the former three spectra follow the pH dependence of Mb^+ at $T = 293$ K, the latter four spectra the temperature dependence at pH = 11.3. Increasing the pH induces discontinuous protein changes between different conformations (Yamamoto, 1997), distinct from substates (Frauenfelder et al., 1988). Because the visible absorption spectra are sensitive to only two Fe-heme states, we assume that these subtle changes pertain to the axial symmetry of the Fe-heme, due to proton titration of the distal and proximal histidines.

Theoretical simulation of the spectra

For the Fe-heme conformations in ferric myoglobin to be investigated, a preliminary study of spin effects on the XANES following thermal spin equilibrium in Mb^+OH^- is essential. We already faced this task in a previous study (Della Longa et al., 1998) using spin-resolved multiple scattering simulations. According to the simulations, conformational effects and spin effects are both present (i.e., experimentally unresolvable) in the range 7111–7130 eV, including the absorption threshold and peak A, while purely structural effects are expected in the range 7130–7170 eV (including peak C_2). For this reason we consider peak C_2 an experimental marker of the symmetry changes in the Fe coordination sphere of metmyoglobin, rather than a spin marker as proposed by Oyanagi et al. (1987).

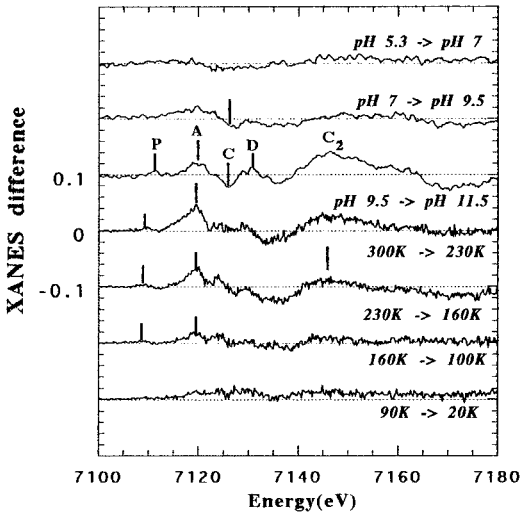

FIGURE 3 XANES difference spectra of Mb^+. As indicated in the figure, from top to bottom, the former three spectra follow the pH dependence of Mb^+ at $T = 293$ K, while the latter four spectra follow its temperature dependence at pH = 11.3.

Spin-resolved MS calculations of the XANES spectra giving best fit to HS Mb^+OH_2, HS Mb^+OH^-, and LS Mb^+OH^- are reported in Fig. 4. The polarized calculations, in which contributions to the XANES signal from heme scattering (*dashed curve*) and axial scattering (*plotted curve*) are separately computed, allow evidentiating the axial contributions to the XANES changes. On the center frame the structures corresponding to best fitting are depicted. The final simulations are obtained by a standard procedure including a weighted sum of the polarized spectra, a convolution with an energy-dependent broadening function, and normalization and alignment to the experimental one, as described in the Methods section. The spin state at the Fe site has been taken into account in the calculations (Della Longa et al., 1998). On the right frame, the best fitting XANES theoretical spectra (*plotted curves*) and the experimental spectra (*circles*) are superimposed. Table 1 summarizes all the results of the Monte Carlo search. Here are reported the minimum value of the fit index factor F, Min(F), the structural parameters extracted from the fit, and nonstructural parameters also extracted during the fitting procedure, i.e., the energy alignment between the theoretical and the experimental curve; the normalization factor, which is experimentally known with an error of some percent, and the energy broadening factors. The actual fitted values of alignment and normalization for Mb^+OH^- at pH 11 at $T = 293$ K are taken as standard. According to the final alignment, the zero energy (VMT) corresponds to ~7105 eV.

During the Monte Carlo search, the fit improvement initially is dominated by the Fe–O distance parameter; after refining the fit, the sensitivity to Fe-heme displacement and Fe-histidine distance emerges. Angular parameters like histidine rotation are actually ineffective, but should emerge in a more refined search. Some of the F vs. parameter diagrams built up during the Monte Carlo XANES search are reported in Fig. 5. Only diagrams corresponding to HS and LS Mb^+OH^- are reported for clarity. The statistical distance errors are evaluated as half-maximum dispersion among values found within an allowable error of 10^{-3} around Min(F). They range between 0.03 and 0.1 Å. According to the final simulations, the Fe-heme displacement from the mean porphyrin plane in Mb^+OH_2 is 0.37 ± 0.05 Å, with the water oxygen at 2.06 ± 0.05 Å and the proximal histidine at 2.11 ± 0.10 Å. In HS Mb^+OH^-, the Fe-heme displacement reduces to 0.25 ± 0.05 Å, with the hydroxyl oxygen at 1.93 ± 0.05 Å. In LS Mb^+OH^-, the Fe is in-plane, 0.08 ± 0.04 Å, and the Fe–O distance is 1.84 ±

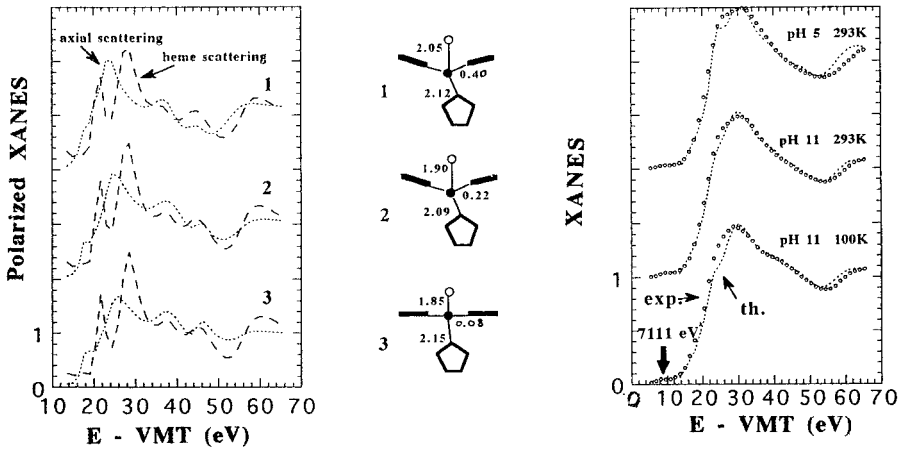

FIGURE 4 *Left frame:* spin-resolved simulation of the XANES spectra of met-myoglobin. Axial scattering (*plotted curve*) and heme scattering (*dashed curve*) are separately calculated to put in evidence the contribution of the structure of the axial moiety on the spectrum. *Center frame:* structures giving best fit to the experimental spectra. *Right frame:* superimposition of theoretical spin-resolved XANES (*plotted curve*) and experimental XANES (*circles*).

0.03 Å. The proximal histidine seems to follow the iron movement.

DISCUSSION

Despite the fact that the XANES theory still cannot be evoked as an exact method to quantitatively measure structural parameters, it seems that the origin of the spectral changes depending on pH and temperature can be understood in structural terms by this method, allowing connection, for the first time, of a large body of experiments from different, unrelated techniques.

Fig. 6 shows the XANES derivative spectra of sperm whale ferric myoglobin at pH 7 and pH 11. These data, compared with those of Fig. 2 *B*, show that the Fe-heme structural changes in horse and sperm whale myoglobin depending on pH are almost identical. Moreover, the comparison between our data on horse Mb^+OH^- at low temperature and that reported for sperm whale (Oyanagi et al., 1987) show the same Fe-heme structural changes depending on temperature. In other words, the same main Fe-heme conformations exist in sperm whale and horse myoglobin, possible differences pertaining only to the pH and temperature kinetics but not the structure of the purely high- and low-spin forms in solution. Here follows a more detailed discussion on each main state of Mb^+.

TABLE 1 Monte Carlo XANES fit on horse Mb^+

Value	pH 5.3, 293 K	pH 11.3, 293 K	pH 11.3, 100 K
Min (F) ($\times 10^2$)	4.03	2.77	2.96
Alignment (eV)	+0.8	0.0	−0.7
Normalization const.	1.02#	1.0	1.0
d(Fe-O) (Å)*	2.06 ± 0.05	1.93 ± 0.05	1.84 ± 0.03
d(Fe-Nϵ) (Å)*	2.11 ± 0.10	2.07 ± 0.05	2.14 ± 0.10
d(Fe-Cp) (Å)*	0.37 ± 0.05	0.25 ± 0.05	0.08 ± 0.04

Phases: Self-consistent spin-resolved (6-coordinated Fe^{3+} in plane) (first occupied energy level − VMT energy) ≈ 6 eV. Broadening: core hole + Instrum. resol. = (2.2 ± 0.3) eV. Energy-dependent part with 2 plasmons at (18.0 ± 0.5) eV − amplitude = (1.5 ± 0.7) eV and (26.0 ± 2.0) eV − amplitude = (2.6 ± 1.0) eV.

*Bond distances are averaged between values found within an allowable error of 10^{-3} around Min(F). Statistical errors are estimated as half maximum dispersion among these values.

HS Mb^+OH_2

The Fe site structure in horse Mb^+OH_2 extracted from our simulations includes a hexacoordinated Fe atom displaced from the heme plane with a small axial asymmetry. The same conformation is found in sperm whale Mb^+OH_2. These results have to be compared with XRD experiments reporting differences at the Fe site between horse and sperm whale Mb^+ at pH 6 (Takano, 1977; Evans and Brayer, 1988). Because no difference is seen in solution, these results could be explained by crystal forces or protocol differences in crystal growing, affecting the unstable equilibria between the Fe-heme local states. Our results fully agree with the Fe-heme conformation reported by Takano (1977), having a Fe atom out of the heme plane by ~0.4 Å toward the proximal histidine. The XANES sensitivity to the Fe-heme displacement, assessed in the present work from theoretical calculations, has been experimentally confirmed in the case of photolysed MbCO under continuous illumination at low temperature (Della Longa et al., 1994). The estimated Fe-heme displacement in photolysed MbCO was ≈0.3 Å, intermediate between the in-plane position of MbCO and the out-of-plane (≈0.45 Å) position of deoxyMb, in good agreement with the latter XRD determination by Schlichting et al. (1994) and Teng et al. (1994).

HS Mb^+OH^-

There is no report about the Fe-heme conformation in met-myoglobin at pH 11. According to our simulated XANES, in HS Mb^+OH^- the iron displacement from the heme plane is reduced to ~0.2 Å, and the distance Fe–O is reduced to 1.9 Å. According to the model of Caughey (1967) we assume the sixth ligand in HS Mb^+OH_2 to be always OH^-, the second proton coming from the hydrogen-bonded distal histidine. The rupture of this hydrogen bond, at pH > 9, should destabilize the hydroxyl ion position

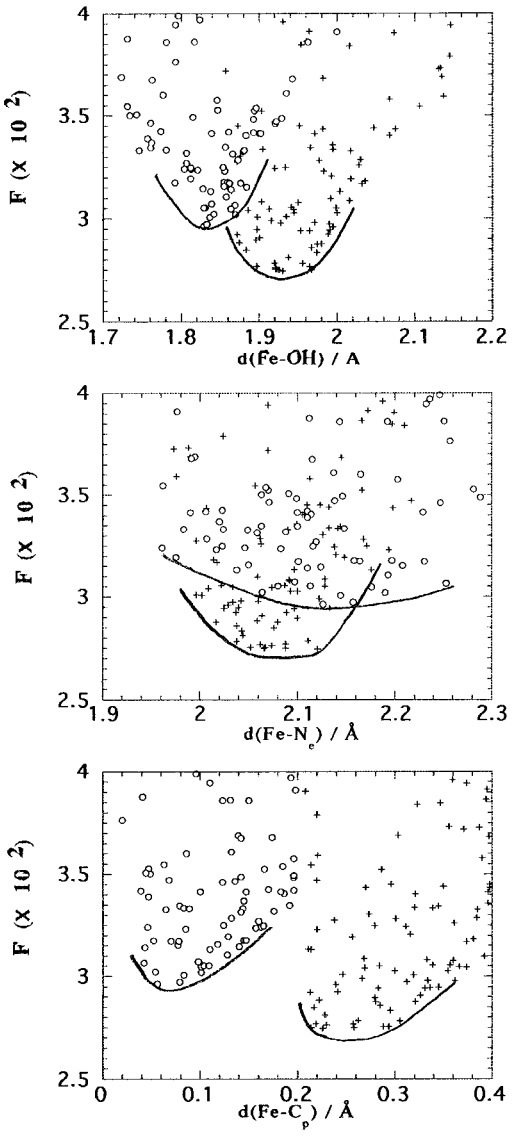

FIGURE 5 [Fit index] vs. [fitting parameter] diagrams built up after iterative improvement by Monte Carlo XANES search. Distance and errors are found within an allowable error of 10^{-3} of the fit index in each diagram.

(2.05 Å apart from the Fe atom), due to both a partial electron density transfer from the hydrogen atom donor toward the Fe-heme–OH^- and a readjustment of the Coulomb electrostatic potential, leading to a shorter bond (1.9 Å) and to a movement of the Fe atom toward the heme plane.

This adduct is in thermal spin equilibrium: according to our description, the partial movement of the iron toward the heme plane going from Mb^+OH_2 to HS Mb^+OH^- would reduce the energy required to move the iron atom further onto the heme plane under spin transition. The roughly estimated work ΔH needed to move the iron toward the heme plane in a Newtonian elastic approximation depends quadratically on the Fe displacement. According to Champion (1989), it can be evaluated as $\Delta H \approx 8.8$ KJ/M for a Fe displacement of 0.4 Å and $\Delta H \approx 2.2$ KJ/M for a Fe displacement of 0.2 Å. This last value is close to the thermodynamic energy difference between spin states according to a Boltzmann distribution model, which is $\Delta G = 1$ KJ/M (Beetlestone and George, 1964).

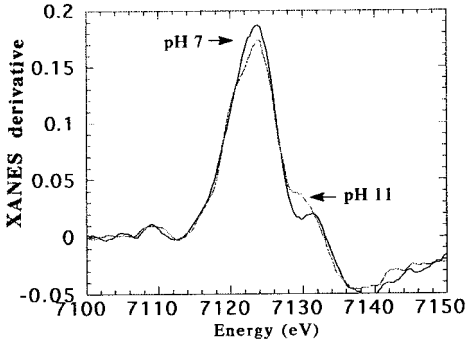

FIGURE 6 XANES derivative spectra of sperm whale Mb^+ at pH 7 and pH 11, $T = 300$ K.

LS Mb^+OH^-

The only structural data on LS Mb^+OH^- come from EPR spectroscopy. Characteristic reported g values at 2.59, 2.17, and 1.83 indicate a Fe-heme conformation with high tetragonal field ($\Delta/\lambda \approx 6$) and high rhombicity ($V/\Delta \approx 0.8$), indicating a highly distorted geometry around the Fe atom. According to the XANES simulations, in LS Mb^+OH^- the Fe octahedral coordination has a marked axial asymmetry, the Fe atom being nearly in the heme plane. The proximal histidine seems to follow the movement of the Fe atom, going from HS Mb^+OH^- to LS Mb^+OH^-, as well as going from Mb^+OH_2 to HS Mb^+OH^-. It should correspond to the functionally relevant movement in hemoglobin: the iron movement is transmitted almost unvaried to the proximal histidine.

Noticeably, this latter Fe-heme conformation extracted from the XANES simulations resembles that reported by XRD on sperm whale MbO_2 (Phillips, 1980; Protein Data Bank code 1MB0). In MbO_2 d(Fe–O) = 1.83 Å, d(Fe–N_ϵ) = 2.07 Å, d(Fe–N_p) = 1.96 Å, and the Fe lies in the heme plane. This structural similarity is well confirmed by the observed spectroscopic similarity between the XANES of MbO_2 (Pin et al., 1994a and references therein) and LS Mb^+OH^-. The spectroscopic similarity can be explained only by 1) a close structural analogy between the Fe site in MbO_2 and that in Mb^+OH^-; and 2) similar electron scattering properties of the axial ligands O_2 and OH^-. Despite the fact that in-phase electron scattering from outer atoms of the sixth ligand is important in many cases, it should be negligible both in MbO_2, due to the large Fe–O–O bending angle (~115°, Phillips, 1980; Protein Data Bank code 1MB0; Congiu-Castellano, 1987), and in Mb^+OH^-, due to the weak electron density of hydrogen.

The analogy between Mb^+OH^- and MbO_2 recalls the long-standing question about the iron net charge in oxy-hemoproteins (Weiss, 1964). The Fe K-edge of MbO_2 is well aligned to that of ferric compounds (Pin et al., 1994a and references therein), so that the oxy-hemoproteins MbO_2 and HbO_2 are assigned by XANES to Fe(III) complexes rather than Fe(II) complexes. This is in agreement with various other spectroscopic data, the most convincing of which (Potter et al., 1987) is the measured O–O stretching band of ^{18}O-substituted analogs ($\approx$1107 cm^{-1}) of myoglobin and hemoglobin, typical of a coordinated superoxide anion, i.e., a $Mb^+O_2^-$ compound. According to this description, antiferromagnetic coupling between the unpaired electrons of the LS Fe(III) atom and the O_2^- ion leads to a diamagnetic compound.

In conclusion, XANES spectroscopy, able to investigate sample solutions at any environmental condition, allows one to gain insight into the main conformations of the Fe-heme in horse and sperm whale ferric myoglobin, obtained by opportunely modulating the pH and temperature equilibria. Three structural states of the Fe-heme, corresponding to HS Mb^+OH_2, HS Mb^+OH^-, and LS Mb^+OH^- can be identified experimentally. The Fe-heme conformations in sperm whale and horse Mb^+ are essentially the same. XANES simulations in the frame of the multiple scattering approach have been carried out to extract the corresponding Fe-heme structures. The chemical transition between Mb^+OH_2 and HS Mb^+OH^-, and the spin transition of Mb^+OH^-, are accompanied by changes of the Fe coordination sphere due to its movement toward the heme plane, coupled to an increase of the axial asymmetry. The Fe-heme structure in Mb^+OH_2 extracted by XANES simulations is in agreement with the XRD structure of sperm whale Mb^+ by Takano (1977) reporting the Fe atom out of the heme plane by $\sim$0.4 Å with a small axial asymmetry of the hexacoordinated iron. The Fe-heme structure in HS Mb^+OH^- extracted from XANES simulation includes a Fe atom closer to the heme plane ($\sim$0.2 Å). This partial movement could contribute to reducing the energy difference between Fe spin states giving thermal spin equilibrium in Mb^+OH. The Fe-heme structure in LS Mb^+OH^- extracted from XANES simulation resembles that of MbO_2, with the Fe atom in the heme plane and a marked axial asymmetry. This fact is in line with the large similarity observed between the experimental XANES spectra of LS Mb^+OH^- and MbO_2, which supports previous assignments of oxy-Mb to Fe(III) antiferromagnetically coupled $Mb^+O_2^-$.

Structural information has been provided by studying the multiple scattering (MS) components in XAS. Support to the present XANES analysis could be given by MS-EXAFS analysis, already applied with some success to probe angular parameters in inorganic complexes (Filipponi et al., 1991; Westre et al., 1994). Because the MS-EXAFS analysis includes the low energy interval, i.e., the LFIR region between 7150 and 7180 eV that we found to variate with pH and temperature, conformational changes would certainly emerge from such an analysis. The measure of the detailed changes in length and collinearity of the 3-body photoelectron pathways Fe–$N_p^{(1)}$-$N_p^{(2)}$-Fe ($N_p^{(1)}$, $N_p^{(2)}$ being opposite pyrrolic nitrogens with respect to the Fe atom), and Fe–O–N_{his}–Fe, is a goal for another independent study.

The authors are indebted to Prof. A. Congiu-Castellano and Prof. A. Bianconi for helpful discussions and for giving access to fast computer facilities. Thanks are due to Dr. G. Bardelloni, Dr. M. Girasole, and Dr. A. Valletta for their help in setting up the MC-XANES package on the IBM-RISC 6000 work station.

This work was supported by grants from CNR (Biotechnologies), Italy, and the INTAS-94-3899 program.

REFERENCES

Ansari, A., J. Berendzen, D. Braunstein, B. R. Cowen, H. Frauenfelder, M. K. Hong, I. E. T. Iben, B. Johnson, P. Ormos, T. B. Sauke, R. Scholl, A. Schulte, P. J. Steinbach, J. Vittitow, and R. D. Young. 1987. Rebinding and relaxation in the myoglobin pocket. *Biophys. Chem.* 26: 337–355.

Antonini, E., and M. Brumori. 1971. Hemoglobin and myoglobin in their reactions with ligands. North-Holland Publ. Co., London. 27:541–548.

Asher, S. A., and T. M. Shuster. 1979. Resonance Raman examination of axial ligand bonding and spin-state equilibria in metmyoglobin hydroxide and other heme derivatives. *Biochemistry*. 18:5377–5387.

Beetlestone, J., and P. George. 1964. A magnetic study of equilibria between high and low spin states of metmyoglobin complexes. *Biochemistry*. 3:707–714.

Bersuker, I. B., and S. S. Stavrov. 1988. Structure and properties of metalloporphyrins and hemoproteins: the vibronic approach. *Coord. Chem. Rev.* 88:1–68.

Bianconi, A., A. Congiu-Castellano, P. J. Durham, S. S. Hasnain, and S. Phillips. 1985. The CO bond angle of carboxymyoglobin determined by angular-resolved XANES spectroscopy, *Nature*. 318:685–687.

Bratkovsky, A. M., S. N. Rashkeev, A. V. Smirnov, and G. Wendin. 1994. Universality in electronic structure and EELS spectra of FeB and NiB crystalline and amorphous systems. *Europhys. Lett.* 26:43–49.

Caughey, W. S. 1967. Porphyrin proteins and enzymes. *Annu. Rev. Biochem.* 36:611–644.

Champion, P. M. 1989. Resonance Raman and site-directed mutagenesis studies of myoglobin dynamics. *In* Protein Structure and Engineering. O. Jardetzky, editor. Plenum Press, New York. 347–354.

Chance, M. R., L. J. Parkhurst, L. Powers, and B. Chance. 1986. Movement of the Fe with respect to the heme plane in the R-T transition of carp hemoglobin. *J. Biol. Chem.* 261:5689–5692.

Chance, M. R., L. M. Miller, R. F. Fischetti, E. Scheuring, W. X. Huang, B. Sclavi, H. Yang, and M. Sullivan. 1996. Global mapping of structural solutions provided by the extended x-ray absorption fine structure *ab initio* code FEFF 6.01: structure of the cryogenic photoproduct of the myoglobin-carbon monoxide complex. *Biochemistry*. 35:9014–9023.

Congiu-Castellano, A. 1987. Oxygen binding site structure in hemoproteins by XANES. *In* Biophysics and Synchrotron Radiation. A. Bianconi and A. Congiu-Castellano, editors. Springer Series in Biophysics, Vol. 2. Springer, Berlin-Heidelberg-New York. 89–93.

D'Alba, G., P. Fornasini, F. Rocca, and S. Mobilio. 1990. Temperature dependence of the EXAFS Debye-Waller factors of AgI. *In* Conf. Proc. Vol. 25 2nd Eur. Conf. on Progress in X-ray Synchrotron Radiation Research. A. Balerna, E. Bernieri, and S. Mobilio, editors. SIF, Bologna. 801–804.

Della Longa, S., I. Ascone, A. Fontaine, A. Congiu-Castellano, and A. Bianconi 1994. Intermediate states in ligand photodissociation of carboxymyoglobin by dispersive x-ray absorption. *Eur. Biophys. J.* 23: 330–335.

Della Longa, S., A. Bianconi, L. Palladino, B. Simonelli, A. Congiu-Castellano, E. Borghi, M. Barteri, M. Beltramini, G. P. Rocco, B. Salvato, L. Bubacco, R. S. Magliozzo, and J. Peisach. 1993. A XANES

study of metal coordination in Co(II)-substituted *Carcinus maenas* hemocyanin. *Biophys. J.* 65:2680–2691.

Della Longa, S., M. Girasole, A. Congiu-Castellano, A. Bianconi, A. P. Kovtun, and A. V. Soldatov. 1998. Spin-resolved x-ray absorption near edge structure (XANES) of metmyoglobin. *Eur. Biophys. J.* 27:541–548.

Della Longa, S., A. Soldatov, M. Pompa, and A. Bianconi. 1995. Atomic and electronic structure probed by x-ray absorption spectroscopy: full multiple scattering analysis with the G4XANES package. *Comput. Mat. Sci.* 4:199–210.

Doster, W., S. Kusack, and W. Petry. 1989. Dynamic transition of myoglobin revealed by inelastic neutron scattering. *Nature*. 337:754–756.

Durham, P., J. B. Pendry, and C. H. Hodges. 1982. Calculation of x-ray absorption near edge structure, XANES. *Comput. Phys. Commun*. 25: 193–200.

Eaton, W. A., and J. Hofrichter. 1981. Polarized absorption and linear dichroism spectroscopy of hemoglobin. *Methods Enzymol.* 76:175–261.

Evans, S. V., and G. D. Brayer. 1990. Horse heart metmyoglobin. *J. Biol. Chem.* 263:4263–4268.

Filipponi, A., A. Di Cicco, T. A. Tyson, and C. R. Natoli. 1991. Ab initio modelling of x-ray absorption spectra. *Solid State Commun.* 78: 256–262.

Frauenfelder, H., F. Parak, and R. D. Young. 1988. Conformational substates in protein. *Ann. Rev. Biophys. Biophys. Chem*. 17:451–479.

Hartmann, H., F. Parak, W. Steigemann, C. A. Petsko, D. Ringe Ponzi, and H. Frauenfelder. 1982. Conformational substrates in a protein: structure and dynamics of metmyoglobin at 80K. *Proc. Natl. Acad. Sci. USA.* 79:4967–4971.

Iizuka, T., and M. Kotani. 1969. Analysis of thermal equilibrium between high-spin and low-spin states of ferrimyoglobin complexes. *Biochim. Biophys. Acta*. 181:275–286.

Kirkpatrick, S., C. G. Gelatt, Jr., and M. P. Vecchi. 1983. Optimization by simulated annealing. *Science*. 220:671–680.

Kotani, M. 1968. Paramagnetic properties and electronic structure of iron in heme proteins. *Adv. Quantum Chem.* 4:227–265.

Oyanagi, H., T. Iizuka, T. Matsushita, S. Saigo, R. Makino, Y. Ishimura, and T. Ishiguro. 1987. Local structure of heme-iron studied by high-resolution XANES: thermal spin equilibrium in myoglobin. *J. Phys. Soc. Jpn.* 56:3381–3388.

Parak, F., H. Hartmann, K. D. Aumann, H. Reuscher, G. Rennekamp, H. Bartunik, and W. Steigemann. 1987. Low temperature x-ray investigation of structural distributions in myoglobin. *Eur. Biophys. J.* 15: 237–249.

Perutz, M. F. 1979. Regulation of oxygen affinity of hemoglobin. *Annu. Rev. Biochem.* 48:327–386.

Perutz, M. F., H. Muirhead, J. N. Cox, and L. C. G. Goaman. 1968. Three-dimensional Fourier synthesis of horse oxyhaemoglobin at 2.8 Å resolution: the atomic model. *Nature*. 219:131–139.

Phillips, S. E. V. 1980. Structure and refinement of oxymyoglobin at 1.6 Å resolution. *J. Mol. Biol.* 142:531–554.

Pin, S., B. Alpert, A. Congiu-Castellano, S. Della Longa, and A. Bianconi. 1994a. XAS spectroscopy of hemoglobin. *Methods Enzymol.* 232: 266–292.

Pin, S., B. Alpert, R. Cortes, I. Ascone, H. L. Chiu, and S. G. Sligar. 1994b. The heme iron coordination complex in His 64 (E7) Tyr recombinant sperm whale myoglobin. *Biochemistry*. 33:11618–11623.

Pin, S., V. Le Tilly, B. Alpert, and R. Cortes. 1989. XANES spectroscopy sensitivity to small electronic changes: case of carp azidomethemoglobin. *FEBS Lett.* 242:401–404.

Potter, W. T., M. P. Tucker, R. A. Houtchens, and W. S. Caughey. 1987. Oxygen infrared spectra of oxyhemoglobins and oxymyoglobins. Evidence of two major liganded O_2 structures. *Biochemistry*. 26: 4699–4707.

Schlichting, I., J. Berendzen, G. N. Phillips, and R. M. Sweet. 1994. Crystal structure of photolysed carbonmonoxy-myoglobin. *Nature*. 371:808–812.

Takano, T. 1977. Structure of myoglobin refined at 2.0 Å resolution. *J. Mol. Biol.* 110:537–568.

Teng, T.-Y., V. Srajer, and K. Moffat. 1994. Photolysis-induced structural changes in single crystals of carbonmonoxy myoglobin at 40 K. *Nature Struct. Biol.* 1:701–705.

Weiss, J. J. 1964. Nature of the iron-oxygen bond in oxyhaemoglobin. *Nature*. 202:83–84.

Westre, T. E., A. Di Cicco, A. Filipponi, C. R. Natoli, B. Hedman, E. I. Solomon, and K. O. Hodgson. 1994. Determination of the Fe–N–O angle in {FeNO}7 complexes using multiple scattering EXAFS analysis by GNXAS. *J. Am. Chem. Soc.* 116:6757–6762.

Yamamoto, Y. 1997. ^{1}H-NMR study of inter-segmental hydrogen bonds in sperm whale and horse apomyoglobins. *Eur. J. Biochem.* 243:292–298.

Yonetani, T., T. Iizuka, and M. R. Waterman. 1971. Studies on modified hemoglobins. *J. Biol. Chem.* 246:7683–7689.